Original Article

JCBFM

Journal of Cerebral Blood Flow & Metabolism
2016, Vol. 36(11) 1965–1977

DOI: 10.1177/0271678X15612779
jcbfm.sagepub.com
SAGE

Regulation of cerebral metabolism during cortical spreading depression

Delphine Feuerstein[1], Heiko Backes[1], Markus Gramer[1], Masatoshi Takagaki[2], Paula Gabel[1], Tetsuya Kumagai[2] and Rudolf Graf[1]

Abstract

We analyzed the metabolic response to cortical spreading depression that drastically increases local energy demand to restore ion homeostasis. During single and multiple cortical spreading depressions in the rat cortex, we simultaneously monitored extracellular levels of glucose and lactate using rapid sampling microdialysis and glucose influx using 18 F-fluorodeoxyglucose positron emission tomography while tracking cortical spreading depression using laser speckle imaging. Combining the acquired data with steady-state requirements we developed a mass-conserving compartment model including neurons and glia that was consistent with the observed data. In summary, our findings are: (1) Early breakdown of glial glycogen provides a major source of energy during increased energy demand and leaves 80% of blood-borne glucose to neurons. (2) Lactate is used solely by neurons and only if extracellular lactate levels are >80% above normal. (3) Although the ratio of oxygen and glucose consumption transiently reaches levels <3, the major part (>90%) of the overall energy supply is from oxidative metabolism. (4) During cortical spreading depression, brain release of lactate exceeds its consumption suggesting that lactate is only a circumstantial energy substrate. Our findings provide a general scenario for the metabolic response to increased cerebral energy demand.

Keywords

Spreading depression, glucose, lactate, glycogen, rapid sampling microdialysis, positron emission tomography

Received 22 December 2014; Revised 25 August 2015; Accepted 8 September 2015

Introduction

Understanding how the brain works and how its activity is supported metabolically has been a major challenge. In particular, the regulation of energy substrate fluxes during periods of increased energy demand, i.e. of functional activation, is still puzzling. There is notably controversial discussion about the main substrate(s) used for ATP production: whether blood-borne glucose is the sole energy substrate in most situations as long claimed,[1] whether cellular trafficking of lactate provides a significant amount of ATP,[2] or whether an under-estimated energy storage readily available in the form of brain glycogen plays an important role.[3] If more than one pathway is presumably used, it is unclear under which circumstances, one or the other will be preferentially activated, what the time sequence of the different pathways to ATP production is, and whether or not there are cellular differences. To address these issues, there is a need for in vivo data that encompass several aspects of brain metabolism simultaneously, and in the same experimental model.

In this study, we analyzed changes in energy substrate fluxes induced by cortical spreading depressions (CSDs), which cause a massive increase in energy demand both under physiological conditions and after brain injury.[4,5] A CSD is a transient simultaneous depolarization of all local cells—neurons and glia.[6,7] Subsequent restoration of ion homeostasis is achieved by an increased activity of transmembrane ATPase ion pumps. This active ion transport is highly dependent on the delivery of energy substrates

[1]Multimodal Imaging of Brain Metabolism, Max Planck Institute for Metabolism Research, Cologne, Germany
[2]Department of Neurosurgery, Osaka University Graduate School of Medicine, Osaka, Japan

Corresponding author:
Heiko Backes, Max Planck Institute for Metabolism Research, Gleueler Str. 50, Cologne, Germany.
Email: backes@nf.mpg.de

for production of ATP, and any reduction in blood supply compromises CSD recovery and prolongs the depolarization.[8] Here, we combined rapid sampling microdialysis (rsMD) and laser speckle imaging (LSI) with positron emission tomography (PET) to simultaneously monitor extracellular glucose and lactate concentrations, local cerebral blood flow (CBF), and [18F]-2-fluoro-2-deoxy-D-glucose (FDG) uptake during single and multiple CSDs in the rat cortex. rsMD measures extracellular glucose and lactate concentration changes with a time resolution of 1 min.[9] Total influx of glucose from blood to tissue can be derived from the time-dependent uptake of FDG quantitatively measured by dynamic PET.[10] Local blood flow changes tightly coupled to CSDs can be measured using LSI at a sub-second time resolution.[11] Combination of the methods provided information about temporal changes in total glucose influx (FDG-PET) and two compartments of the metabolic pathway (extracellular glucose and lactate, rsMD) while the timing of CSD occurrence was derived from LSI.[12] Based on the combined and simultaneously acquired data and on steady-state conditions, we developed a mass-conserving compartment model with linear transfer constants that is able to explain the observed dynamic fluxes of energy substrates. The patterns of substrate fluxes during CSD provide a general realistic scenario for the response of cerebral tissue to any physiological increase in energy demand, i.e. to any type of cerebral functional activation that is ATP-demanding.

Materials and methods

Surgical procedures

All animal procedures were performed in accordance with the German regulations for animal protection (TierSchG, 2006) and were approved by the local animal care committee and local governmental authorities (LANUV NRW) and written up following the ARRIVE guidelines. Fifteen male Wistar rats (Janvier, France; weight: 300 to 420 g; age 9 to 12 weeks; housed with an inverse 12 h day–night cycle with lights on at 8:30 pm in a temperature ($22 \pm 11^{\circ}C$) and humidity ($55 \pm 5\%$) controlled room pairwise in type-4 cages filled with Lignocel; experiments performed between 9 am and 4 pm) were anesthetized with isoflurane (induced with 5% and maintained with 1.5% to 2%) in 70%/30% nitrous oxide/oxygen during surgical procedures. Animals breathed spontaneously, and their body temperature was kept at 37°C using a servo-controlled heating blanket. The left femoral artery was cannulated for continuous monitoring of arterial blood pressure and for hourly measurement of blood gases (arterial PaO_2, $PaCO_2$, pH). Two catheters were inserted in the tail, one for continuous intravenous infusion of propofol and one for bolus injection of FDG. Frontal and parietal bones were exposed and thinned out to transparency using a dental drill. Drilling was performed under continuous saline irrigation to prevent heat injury. The cavity formed yielded a field of view for LSI through thin skull of 12×7 mm^2 that was symmetrical around mid-line. In the left hemisphere, a small burr-hole was drilled into the frontal bone for CSD induction, either by needle prick (single CSD group, $n = 8$) or by epidural KCl application (multiple CSDs group, $n = 7$). Additionally, a small durectomy was drilled in the temporal lobe (3.5 mm posterior and 4 mm lateral to Bregma) for implantation of a microdialysis (MD) probe (MAB 6.14.2, Microbiotech, Sweden).

Multimodal in vivo measurements

At the end of surgery, the animals were positioned on our multimodal imaging holder in the PET gantry.[12] The thinned skull surface was covered with warm paraffin oil, and LSI was started. The MD probe was then slowly implanted (0.5 µm/min) using a piezo-electric motor (M-663, Physics Instruments, Germany) to minimize trauma. The probe laid obliquely with full membrane length (2 mm) in cortex and was perfused at 1.6 µL/min with artificial cerebro-spinal fluid. Dialysate was analyzed for glucose and lactate by rsMD every minute.[9] During pilot and sham experiments, we verified that the presence of the MD probe did neither disturb the propagation of CSD waves nor imaging with LSI or PET.

After LSI baseline imaging and rsMD baseline measurements, propofol infusion was started at 38 mg/kg/h via tail vein. Isoflurane weaned off over 15 min, and propofol concentration (33 to 53 mg/kg/h) was adjusted to keep breathing rate within 60 to 80 cycles/min. Thirty minutes after isoflurane was completely off, systemic variables, CBF and rsMD glucose and lactate concentrations had stabilized.

Two mCi FDG (0.5 mL) were then injected into tail vein. PET scans were started at the time of bolus tracer injection, and emission data were acquired for 90 min. At time $t = 20$ min after tracer injection, either a single CSD wave was induced by a needle prick ($n = 8$) or multiple CSD waves were induced by epidural application of 3 M KCl through a cotton ball for 70 min ($n = 7$) in the left hemisphere. LSI and rsMD measurements continued uninterrupted during the whole PET scan. Animals that showed non-physiological blood pressure or arterial blood gases, unstable CBF in the right hemisphere, or abnormal baseline rsMD concentrations of glucose and lactate were excluded from this study.

Data analysis

Simultaneous LSI and PET imaging were implemented as described elsewhere.[12] Images were co-registered

using our in-house fiduciary marker and the procedure described elsewhere.[12] The position of the MD probe was readily defined on the LSI images, and co-registered regions of interest for LSI (ROIs: 1.9×1.9 mm^2) and volumes of interest for PET (VOIs: 1.9 mm $\times$ 1.9 mm $\times$ 2.4 mm) were analyzed around the tissue sampled by the MD probe. ROIs and VOIs in the corresponding positions in the contralateral hemisphere were also analyzed (Figure 1(a)).

Speckle contrast and inverse correlation time (ICT) were calculated on a 7×7 pixel sliding window using previously published algorithms.[11] Percent changes in CBF were calculated from a baseline ICT value averaged over 5 min prior FDG injection. With LSI, the propagation of the CSD waves on the cortex surface was tracked, as validated in many earlier studies with electrophysiological recordings.[11,13] The typical CBF changes induced by one single CSD wave and by multiple CSD waves are plotted in Figure 1(d) and (b), respectively.

PET images were corrected for attenuation using transmission data from a ^{57}Co source. After histogramming in time frames of 5 min and Fourier rebinning, emission PET data were reconstructed using two-dimensional filtered back-projection. FDG uptake as a function of time (time-activity curve, TAC) for each VOI was calculated by spatial averaging (Figure 1(a)). To investigate the changes in FDG uptake due to CSD propagation in the left hemisphere, we calculated the FDG uptake percent change in the ipsilateral VOI compared to its counter-part contralateral VOI in each animal. Each curve was then normalized by the contralateral VOI to exclude artifacts due to the variability in FDG injection. The resulting FDG uptake curves were then averaged over $n = 8$ animals for the single CSD group and $n = 7$ animals for the multiple CSDs group (Figure 1(c) and (d)).

rsMD data were processed using our noise-removal algorithms described in Feuerstein et al.[14] Dispersion and time delay from the MD probe to the rsMD analyser were accounted for after a calibration in vitro. MD recovery was estimated in vivo by the no-net flux method at steady state (see details in Supplementary material S2). Percent concentration changes were then calculated given baseline concentrations during 5 min prior to CSD induction in each animal. The time-aligned concentration changes were then averaged across all animals within each respective experimental group.

Two-cell type model

We developed a numerical model to calculate substrate fluxes after CSD assuming that substrate kinetics can effectively be described by two cell types. Details, model equations, and further assumptions are given in the Supplementary material S1.

Statistics

All data are reported here as mean values $\pm$ standard error of the mean. For statistical inference only, a 5-min moving average was performed on the rsMD data. FDG normalized TACs, and rsMD glucose and lactate were then treated identically. To verify if all data points before CSD induction were not different from control value (zero), a one-sample t-test was performed at each negative time point. Since there was no significant difference in all cases, a one-way repeated measure analysis of variance (ANOVA) was performed on the time courses of FDG and rsMD for positive time points. Tests for normality (Shapiro–Wilk test) and equal variance (Levene median test) passed. ANOVA was followed by a multiple comparison versus control group (Holm–Sidak method). Statistical significance was inferred from a p value < 0.05.

Results

Metabolic response to multiple CSD waves—experimental data

CSD waves were visualized by LSI as hyperemic waves that propagated in the left hemisphere (Figure 1(a), bottom, solid line ROI). In total, 18 to 24 CSDs propagated during 70 min of KCl application, repeating within 1.7 to 5.2 min (Figure 1(b), bottom). The CSD time occurrence was taken as the average of the hyperemia onset times over all seven animals, ignoring the last 10 min where CSD waves did not propagate in some animals (Figure 1(c), bottom).

During KCl application, FDG uptake was strongly increased in the hemisphere ipsilateral to CSD propagation compared to the contralateral hemisphere (Figure 1(a), left hemisphere), rsMD glucose dropped significantly (Figure 1(b), red) and rsMD lactate increased for a prolonged period of time (Figure 1(b), green). In the contralateral hemisphere, CBF remained stable around baseline levels (Figure 1(b), bottom, dashed line). Under the assumption that glucose consumption also remains stable, FDG uptake in the contralateral hemisphere could be regarded as a "control" normal uptake (Figure 1(b), top, dashed line). Before CSD induction, the FDG TACs in ipsi- and contralateral hemispheres were similar (Figure 1(b), top), and differences in FDG uptake between both hemispheres were not significant (Figure 1(b), top, one-sample t-test: $p > 0.05$ for all data points before time $t = 0$). As soon as the first CSD wave reached the ipsilateral VOIs (as seen per LSI, Figure 1(b), bottom,

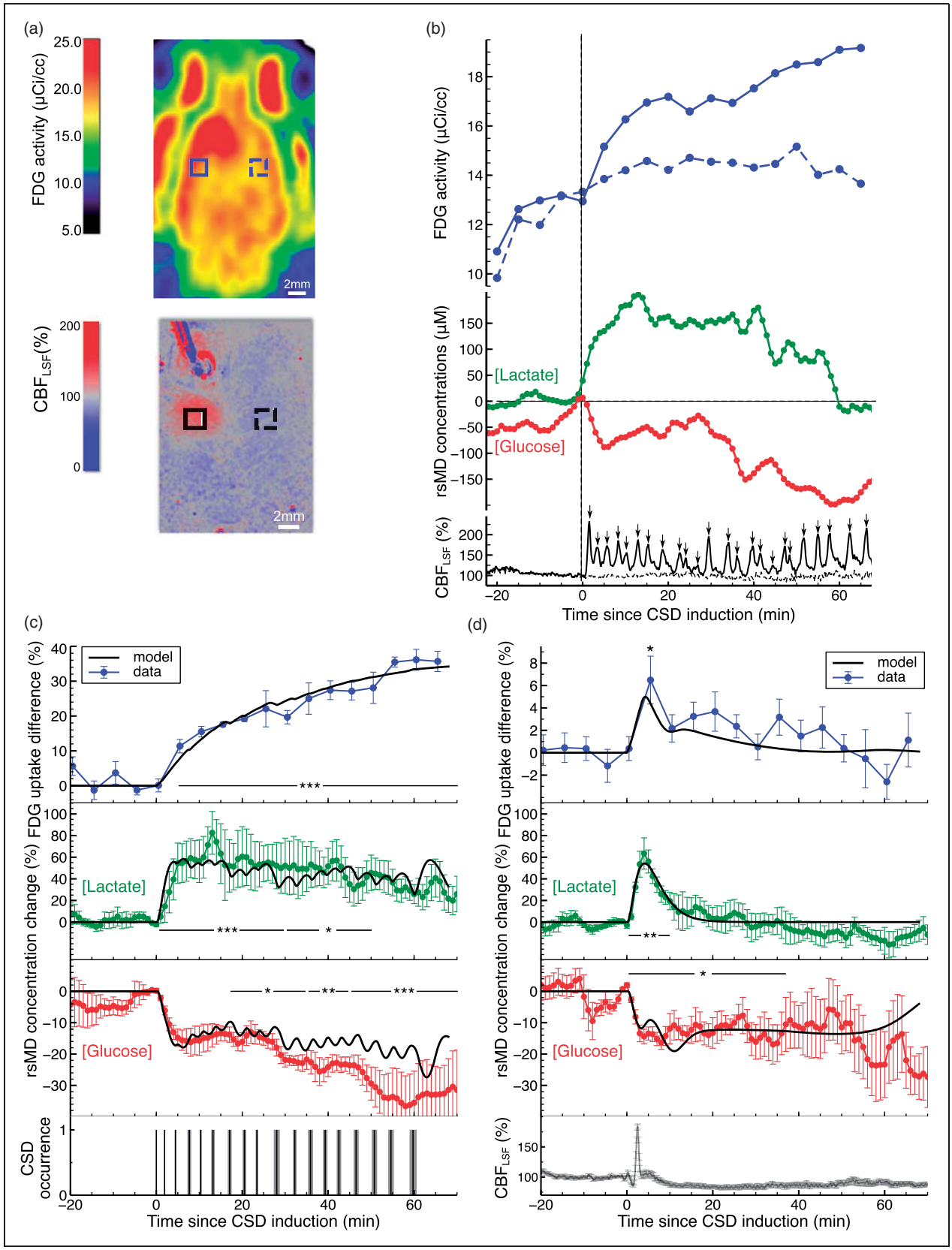

Figure 1. Data acquired during CSD in the rat cortex and comparison to the model output. ((a), top) Horizontal PET image of FDG accumulation over 90 min. Multiple CSDs were induced 20 min after FDG injection. ((a), bottom) LSI image of the same rat while a

(Continue)

solid line), the FDG TAC in the CSD hemisphere departs from the contralateral uptake curve (Figure 1(b), top, solid line). The difference in FDG uptake between both hemispheres increased with the occurrence of further CSDs to a maximum of $+36.2 \pm 3.0\%$ after 70 min (Figure 1(c), top, $F(2,15) = 26.7$, $p < 0.001$ vs. control). In parallel to increased FDG uptake, CSD waves led to ever-decreasing levels of extracellular glucose, down to a minimum of $-36.6 \pm 9.7\%$ compared to baseline (Figure 1(b) and (c), red curve, significant effect of CSD on rsMD glucose: $F(4,13) = 4.1$, $p < 0.001$). Lactate concentrations significantly increased up to $+82.5 \pm 19.8\%$ above baseline levels and declined gradually to $+20\%$ above baseline at 70 min (Figure 1(b) and (c), green curve, significant effect of CSD on rsMD lactate: $F(4,13) = 4.6$, $p < 0.001$).

Metabolic response to single CSD waves—experimental data

One CSD wave caused a transient hyperemia up to $183.9 \pm 12.4\%$ above control CBF (Figure 1(d), bottom). The blood flow levels remained slightly below baseline for the next hour (80% to 90% of baseline). The hyperemic wave corresponded to a transient elevation in FDG uptake in the ipsilateral hemisphere compared to the contralateral hemisphere (Figure 1(d), top). This elevation was small ($+6.5 \pm 2.1\%$) but significant ($F(8,13) = 1.826$, $p = 0.047$). The transient change was followed by a prolonged period of decreased FDG uptake in the ipsilateral hemisphere so that differences between ipsi- and contralateral hemispheres disappeared 32 min after the CSD wave. Similarly, rsMD glucose transiently dropped to a minimum of $-16.4 \pm 2.1\%$ of baseline within the first 10 min of CSD induction (Figure 1(d), red). This was followed by a prolonged period of reduced glucose concentrations stabilizing around -10% of baseline during the next 45 min (significant effect of CSD on rsMD glucose, $F(4,13) = 2.7$, $p = 0.022$). Lactate showed a monophasic transient increase, reaching a maximum of $63.4 \pm 14.5\%$ above baseline at 6 min post-CSD induction before recovering to baseline concentrations within less than 20 min after CSD induction. Although we cannot account for changes in MD recovery during CSD, the concentration changes that we here observe are consistent with other reports. Autoradiography[15] or bioluminescence[16] measured a peak increase in lactate, within 2 min after SD elicitation, to 180% of lactate baseline levels. Here, our MD changes, after steady state in vivo recovery corrections, yielded a peak increase of 163% of baseline lactate level. This is, therefore, very similar to 180% measured by Selman et al.[6] However, others have reported a fourfold increase of cortical lactate,[17] suggesting that we might underestimate the lactate change during CSD, possibly because of a drop in microdialysis recovery during CSD. Furthermore, Mies and Paschen,[18] as well as Selman et al.,[16] both measured cortical glucose concentrations drop of—40% to -50% below baseline values within the first 2 min after the CSD. We here measured -20% decrease, which is in the same order of magnitude but not identical. Would the microdialysis recovery of glucose dramatically drop during the CSD, the glucose concentrations we here report would underestimate the true extracellular glucose concentrations, and therefore amplify the concentration drop after the CSD. However, in comparison to reported values in literature, we seem to slightly overestimate glucose concentrations, thereby suggesting that the likely MD recovery decrease due to the CSD plays a minor role. Hence, the microdialysis concentrations measured here, and corrected by the in vivo recovery at steady state and in vitro dispersion, seem to mirror extracellular concentrations of glucose and lactate, even during CSD. However, we cannot exclude that there is some uncertainty and limitation to reliably quantify the relationship between MD concentrations and tissue concentrations.

Low extracellular glucose levels and subnormal uptake of FDG are consistent with decreased glucose consumption. Thus, it seems that some energy demanding cellular

Figure 1. Continued.
CSD was propagating, inducing a hyperemic wave (passing the square ROI at the time of this still-image). The pipette for CSD induction is visible in the upper left. (b) Data traces recorded in the animal in the ipsi- and contralateral ROIs shown in a: FDG uptake (top), rsMD concentrations of glucose (red) and lactate (green) (middle), and percentage of CBF changes from LSI (bottom). Solid lines are from ipsi-, dashed lines from contralateral ROI. The microdialysis probe was at the site of the ipsilateral ROI. Time 0 is the CSD induction time while FDG was injected at time $t = -20$ min. (c) Average data from animals acquired during multiple CSDs ($n = 7$ animals). LSI data in the lower panel are shown as average CSD occurrence time (black bars) and standard deviation (grey). (d) Average data from animals with a single CSD induced at time 0, 20 min after FDG injection ($n = 8$). Solid black lines overlapped on the average FDG and rsMD data in (c) and (d) show respective theoretical data calculated by the model. In (c) and (d) rsMD data are displayed as difference from baseline just before CSD induction (in percentage of baseline), FDG data as difference between ipsi- and respective contralateral FDG uptake in percentage of the contralateral uptake. FDG: [18F]-2-fluoro-2-deoxy-D-glucose; CBF: cerebral blood flow; rsMD: rapid sampling microdialysis; CSD: cortical spreading depression.

processes (P_x in our model) are impaired for ~1 h after a single CSD. Supportive evidence for this hypothesis is discussed in details in Supplementary material S3.

Concentrations of energy substrates during CSD—theoretical model

Experimental data from multiple and single CSD could be explained by the two-cell type compartment model outlined in Figure 2(a). A detailed description of the theoretical model is available in the Supplementary materials S1 and S2. The output of the model is superimposed on the experimental data in Figure 1(c) and (d) and shows good agreement with all measurements. Resulting kinetic parameters and concentrations are listed in Supplementary Tables S1, S2, and S3. Consequently, concentrations of energy substrates varied with time during single and multiple CSD according to the functions plotted in Figure 2(b) and (c). Shown outputs were derived from our mass-conserving model that complies with observed steady-state concentrations and only reacts to changes in ATP concentrations (see details in Supplementary materials S1, S2). It entails the scenario of substrate fluxes during increased energy demand described hereafter.

ATP consumption and production

Supplying the brain with energy means preserving cellular ATP levels (Figure 2(b) and (c)). At steady state, ATP consumption of 5.6 mM/min (value in agreement with other studies under propofol anesthesia[19]), 3.6 mM/min in neurons and 2.0 mM/min in astrocytes, is matched by ATP production from glycolysis and oxidative phosphorylation (6% vs. 94%)[20] (Figure 3, prior time $t = 0$).

After depolarization of cells by a single CSD, ATP utilization rapidly shoots up (to 10 mM/min ATP in total) to provide energy for active transmembrane ion pumps (described by P_e, see Supplementary material S1). Glycogen breakdown is the first process that provides an essential amount of ATP: within the first 25 s after a CSD, glycogen breakdown contributes to up to 30% of astrocytic ATP formation (Figure 3(b)). Neuronal ATP production peaks only at 45 s post CSD, via increased glycolysis (to a maximum of 18% of neuronal ATP production), followed by increased glucose oxidation.

After recovery from a single CSD, the energy demand for restoration of ion homeostasis returns to normal within 4 min, which is in agreement with observed normalization of intracellular calcium levels.[21] However, the total ATP use remains reduced for up to ~1 h, due to a persistent shut down of energy demanding processes (described by P_x in Supplementary material S1). The tissue reacts to this state of lower energy demand by reducing the net inflow of glucose to the brain (K_1) and reducing ATP production via hexokinase activity (k_3 in the model) and via the tricarboxylic acid (TCA) cycle (k_{OXY} in the model, see Supplementary material S1)

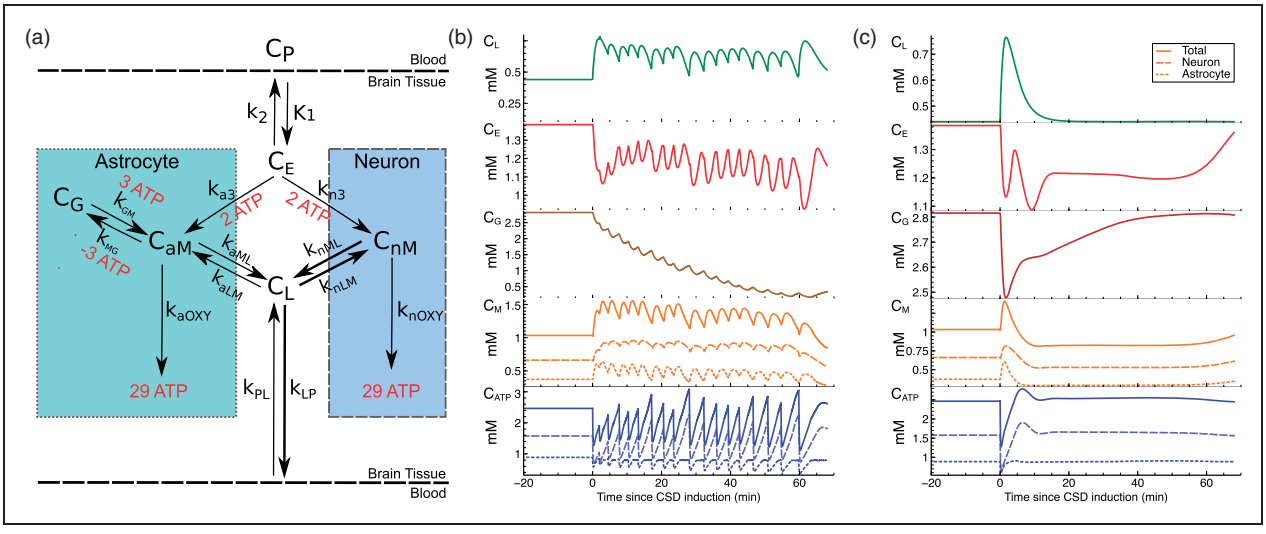

Figure 2. Two-cell type model of brain metabolism. (a) Sketch of simplified glucose and lactate pathways in cerebral tissue. Contributions of reactions to the ATP level are indicated in red. (b) Time courses of concentrations during multiple and (c) single CSD predicted by the model. From top to bottom these are: extracellular lactate (C_L) and glucose (C_E), glycogen (C_G), glucose-6-phosphate (C_M), and ATP (C_{ATP}). Intracellular concentrations are plotted in dashed lines for neurons, in dotted lines for astrocytes while solid are for total. CSD: cortical spreading depression.

such that the net ATP production matches the consumption (Figures 3(b) and 2(c)). A new steady state of decreased energy demand is reached at ~40 min when glycogen storages have been refilled (Figure 2(c)).

In the case of multiple CSDs, the second CSD hits the tissue before the state of low energy demand is reached and again causes an increase in energy demand, which again stimulates increased ATP production via increased glycogen breakdown followed by glycolysis and oxidative phosphorylation (Figure 3(a)). Each CSD reduces the available amount of glycogen, leading to a continuous depletion of glycogen stores (Figure 2(b)). As a consequence, the contribution of glycolysis to peak astrocytic ATP production rises from 8% after the first CSD to 16% after the 16th CSD (compared to 6% at rest), and the peak astrocytic ATP production rate decreases from 4.3 to 3 mM/min when the contribution of glycogen is negligible. In contrast, the peak neuronal ATP production rate is more stable, peaking between 5.7 and 6.5 mM/min in the acute CSD phase, with glycolysis accounting for 18% for the first CSD and 15% for the 10th CSD. In both neurons and astrocytes, ATP is predominantly produced by oxidative phosphorylation (Figure 3).

Oxidative vs. non-oxidative metabolism

Using our model, we calculated the time courses of the cerebral metabolic rate of oxygen (CMR_{O2}) (as the amount of oxidatively metabolized glucose multiplied by six) and CMR_{glc} (rate of phosphorylation of blood-borne glucose to glucose-6-phosphate[22]) during CSD. During the very first minute of increased ATP demand, the CMR_{O2}/CMR_{glc} ratio transiently decreases (<3 in our case, Figure 6). This would be exacerbated in conditions where oxygen supply is limited, as observed by Takano et al.[23] in the mouse cortex during a CSD. However, when glucose-6-phosphate (C_{nM} and C_{aM}, Supplementary material S1) is oxidized, the CMR_{O2}/CMR_{glc} ratio returns to normal and even exceeds the value of ~6 (Figure 6(b)).

Furthermore, we could assess the relative contribution of non-oxidative glycolysis vs. oxidative phosphorylation to the production of ATP. In baseline conditions, 92% of total $C_M = C_{nM} + C_{aM}$ are used for oxidative ATP production in the TCA cycle. Overall, integrated over a 10-min period after a single CSD, only 67% of C_M enters the TCA cycle while at the same time a noticeable amount of lactate is released, indicating a shift from oxidative to non-oxidative ATP

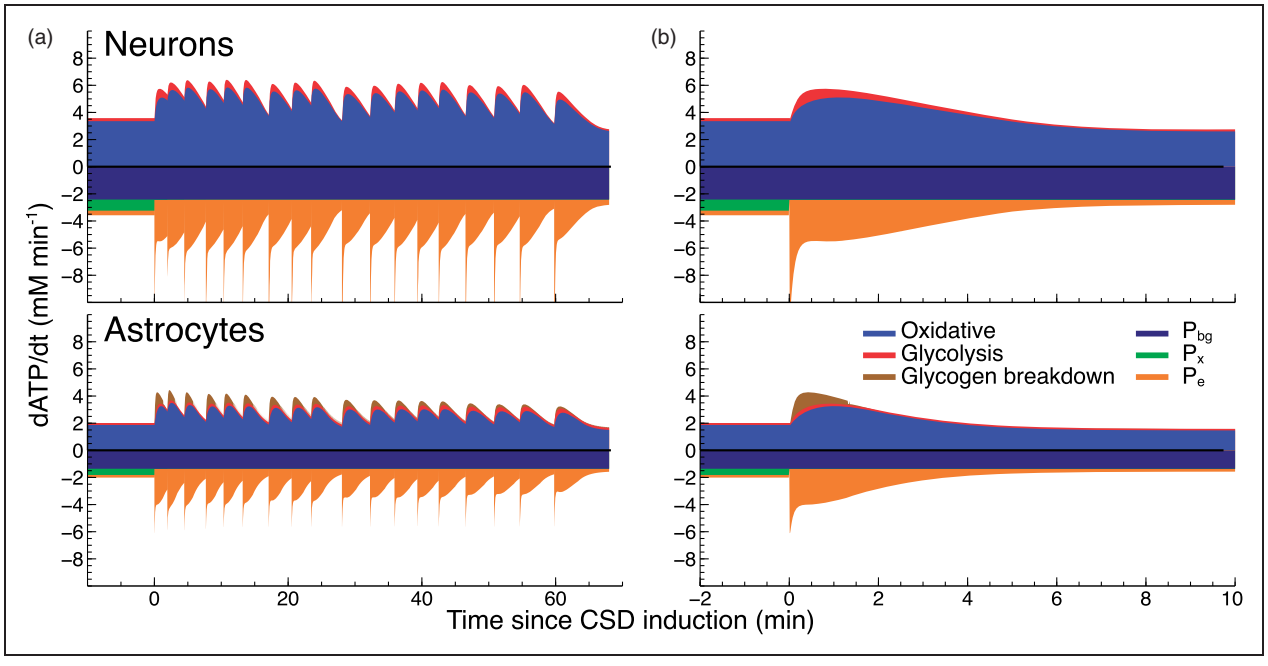

Figure 3. ATP consumption and production rates in neurons and astrocytes during multiple (a) and single CSD (b). Positive values indicate production, negative values consumption of ATP. Processes are added up, so that the colored area represents the amount of ATP produced/consumed by each process and the envelope shows the total ATP production/consumption. ATP is consumed for restoration of ion homeostasis via transmembrane ion pumps (P_e), processes that are shut down for some time after CSD (P_x), and processes that are not influenced by CSD (P_{bg}). ATP is produced by oxidative metabolism, glycolysis, and glycogen breakdown (in astrocytes only). Only the first 10 min after a single CSD are shown in (b), since the new steady state lasts for the subsequent 50 min. All following figures will also focus on these first 10 min after a single CSD. CSD: cortical spreading depression.

production (Figure 4). However, detailed analysis of our data indicates that due to the different efficiencies of glycolysis and oxidative metabolism (2 vs. 29 mol ATP/mol glucose), the changes of pathways have only minor consequences for the sources of ATP production: during CSD 92.4% of ATP is produced via oxidative metabolism vs. 93.5% in baseline conditions. Thus, even when energy demand is high, as caused by CSD, the predominant fraction of ATP is produced by oxidative metabolism.

Sources and sinks for oxidative ATP production

Glucose-6-phosphate (C_M in our model, Figure 2 and Supplementary material S1) plays a pivotal role as branch point in the glucose pathway with several alternative metabolic fates: it can be substrate for generation of ATP by oxidative phosphorylation, substrate for release and/or use of lactate, and substrate for synthesis of glycogen. Additionally, glucose-6-phospate can be used to generate NADPH or precursors for nucleic acid biosynthesis in the pentose phosphate pathway. However, the major fraction of glucose-6-phosphate entering this pathway is recycled to be used for energy production. In our model, we assume that the portion of glucose lost in the pentose phosphate pathway remains constant during CSD (included in the background energy, P_{bg}, Supplementary material S1) (see Figure 3). Apart from blood-borne glucose, lactate and glycogen are potential sources for the precursor pool for oxidative ATP production in the TCA cycle. In order to quantify their relative contributions, we analyzed the sources of C_M (Figure 4). During baseline conditions, blood-borne glucose is the sole source for C_{aM} in astrocytes and the major source for C_{nM} (89%) in neurons. In both cell types, >90% of C_M are used for ATP production by oxidative phosphorylation and <10% of C_M are transformed to lactate (presumably from cellular parts with limited access to mitochondrial ATP).[20,24,25]

In response to a single CSD, there is an increase in neuronal C_{nM} production to nearly 400% of baseline. In astrocytes, C_{aM} production even increases to 800% of baseline but here the main source is glycogen (71% at the peak of C_{aM} production). Note that each glycogen molecule contributes to ATP production in two ways, first by glycogen breakdown (Figure 3) and second by oxidative phosphorylation (Figure 4). A reduction of brain glycogen content during CSD is consistent with other reports.[26,27] Breakdown of glycogen in astrocytes leaves more blood-borne glucose to neurons: at the peak, 80% of total blood-borne glucose influx contribute to neuronal C_{nM} (Figure 4(b)). The rapid increase in ATP consumption in regions with limited access to mitochondrial ATP causes a rise in glycolysis and subsequent lactate production.

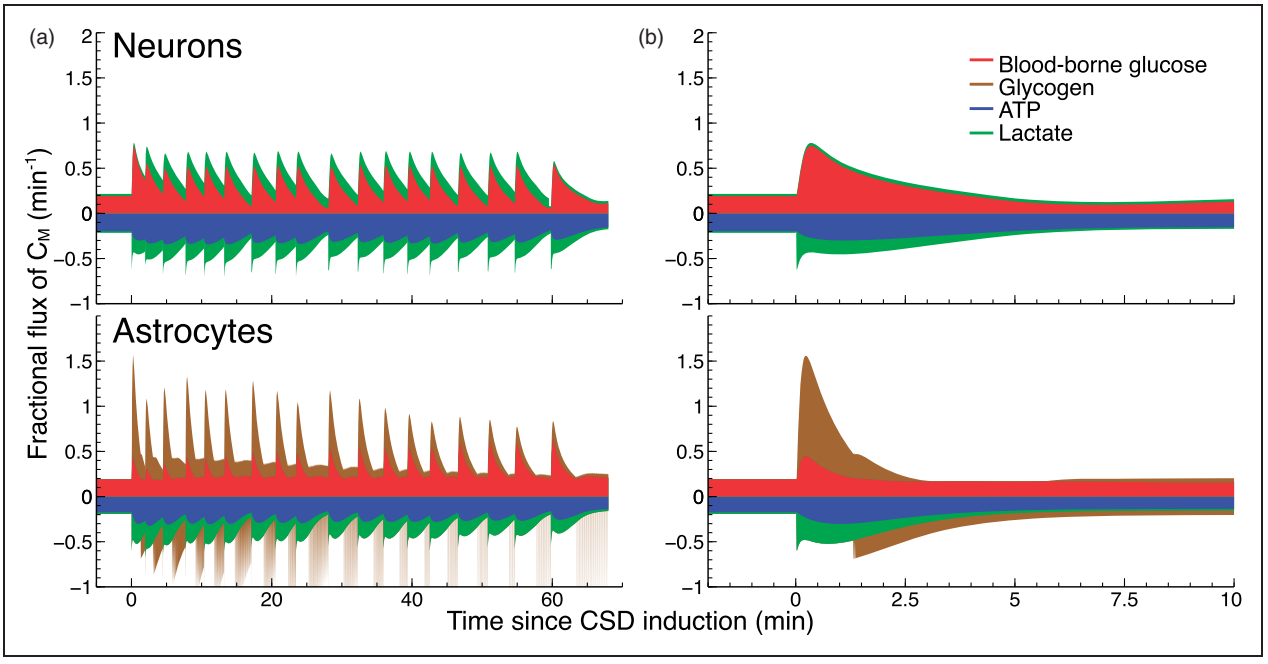

Figure 4. Sources and sinks of glucose-6-phosphate (C_M), the branch point between oxidative energy production (ATP) and other fates of glucose during multiple (a) and single CSD (b). Sources for C_M (positive values) are: blood-borne glucose, lactate (only in neurons), and glycogen (in astrocytes only). Sinks for C_M (negative values) are: ATP, lactate, and glycogen. CSD: cortical spreading depression.

Once cellular ATP levels have been restored, glycogen breakdown stops, lactate production gradually returns to normal, and glycogen stores are totally refilled within 30 min (Figure 2(c)).[28]

In the case of multiple CSDs, the contribution of glycogen to astrocytic C_{aM} production gradually decreases as the stored amount of glycogen decreases with each CSD (Figure 2(b)). As a result, blood-borne glucose becomes gradually the main source of C_{aM}, from 29% to 94% of the total C_{aM} production between the first and last CSD. In response to the 18th CSD, 60% of the total blood-borne glucose influx is used by the neurons, approximately matching the neuron/astrocyte volume ratio in rats (Figure 4(a)). To compensate for the lesser extent of blood-borne glucose available, neurons resort to another source for their ATP production: lactate. However, this usage of lactate, solely by neurons, takes place under particular conditions detailed below.

Lactate production, removal, and utilization

During baseline conditions, a small amount of lactate (0.032 mM/min) is transported from blood to brain, taken up by neurons, and fully oxidized to CO_2.[29] At the same time, 9% of the blood-borne glucose is transformed to lactate and is cleared from brain tissue into the blood stream (at a rate of 0.036 mM/min, Figure 5)[20] causing a small net release of lactate (0.004 mM/min). After CSD, energy need is elevated (in regions with limited access to mitochondrial ATP as well) and lactate release from both neurons and astrocytes increases: more than 50% of C_M are transformed to lactate (Figure 4). In the case of a single CSD, the increased extracellular lactate is cleared into the blood stream at a fast rate of ~0.3 mM/min (Figure 5(b)) and lactate levels return to normal after ~15 min (Figure 1(c) and 2(c)).

In the case of multiple CSDs, another surge for ATP (due to a CSD again spreading into this region of the brain) occurs at a time when extracellular lactate concentration is still at ~180% of baseline. In that case, neurons take up and use lactate as an additional energy substrate (Figure 4(a)). Lactate can then yield up to 70% of total neuronal glucose-6-phosphate (C_{nM}). Simultaneously, neurons also release lactate and, on average, they produce more lactate than they consume, even during times of increased energy demand (Figure 5(a), bottom).

The time course of lactate fate is shown in Figure 5, where sources and sinks of extracellular lactate,

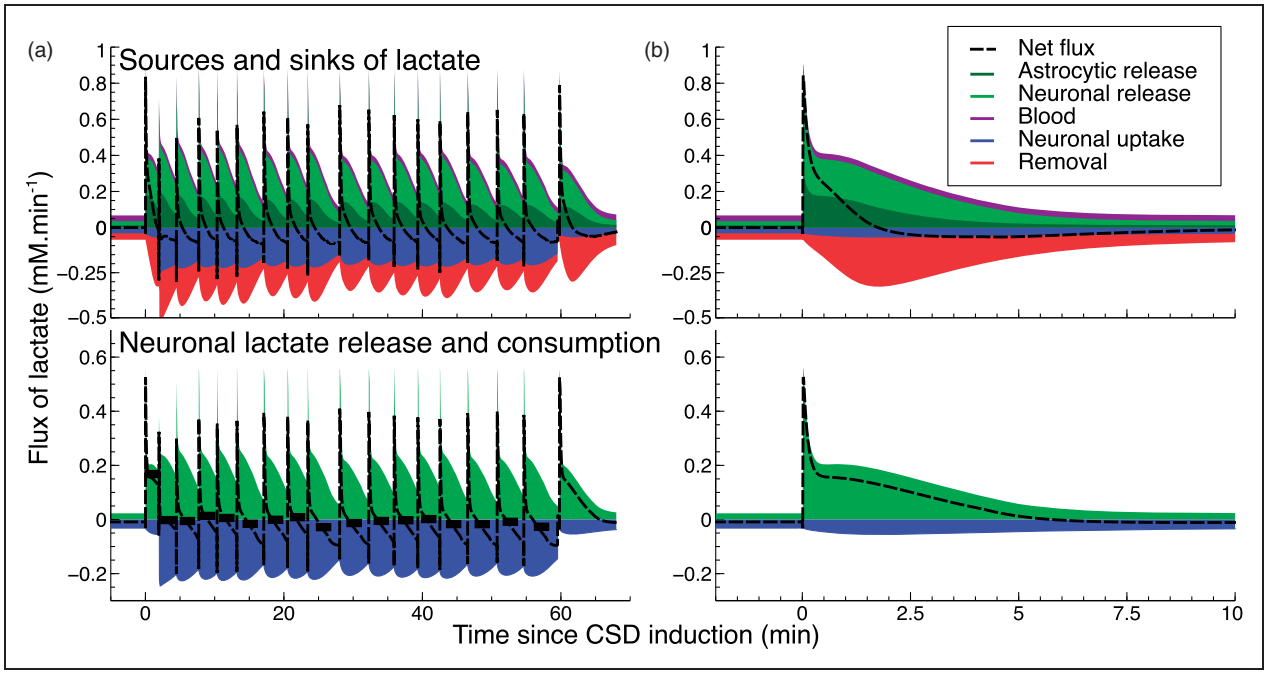

Figure 5. Origin and fate of lactate in cerebral tissue during multiple (a) and single CSD (b). Sources and sinks for extracellular lactate are shown in the top row. During CSD, lactate release from neurons and astrocytes (positive values) is increased. Lactate is either removed to the blood stream or consumed by neurons (negative values). Bottom row figures show neuronal contribution to extracellular lactate. Black rectangles indicate lactate release and removal integrated over time from CSD to start of next CSD. On average, neurons never consume more lactate than they produce. CSD: cortical spreading depression.

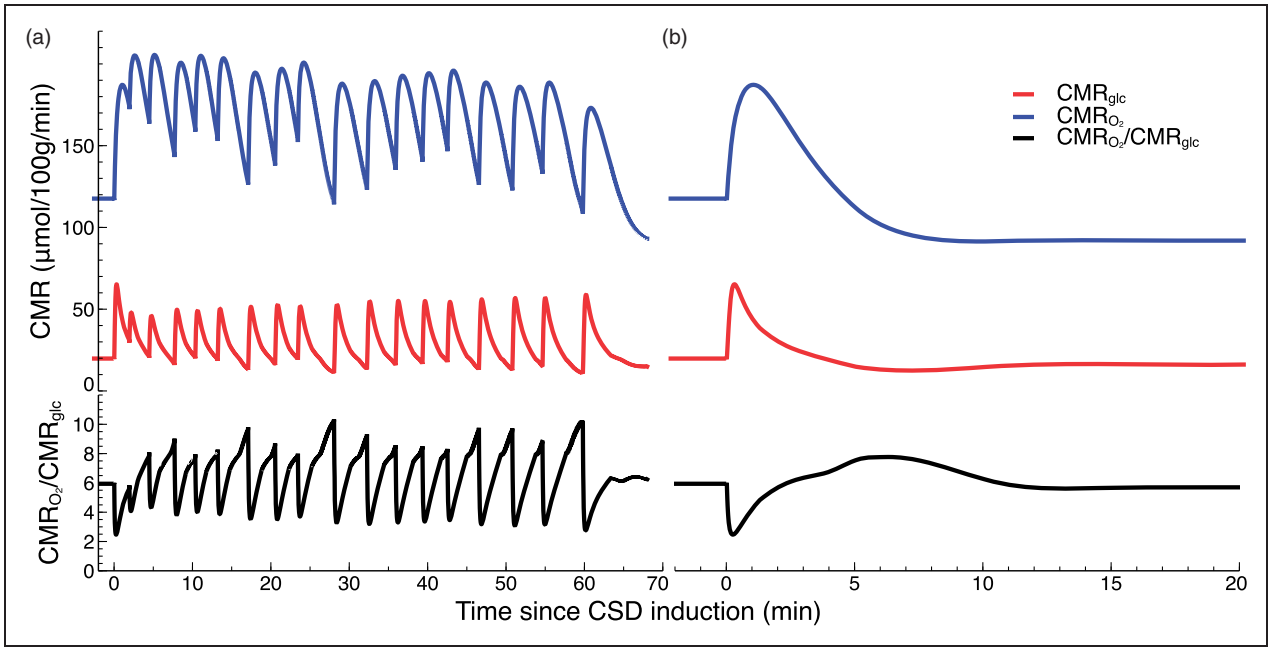

Figure 6. Oxygen consumption rate (CMR_{O2}), glucose consumption rate (CMR_{glc}), and ratio of oxygen to glucose consumption rates as a function of time during multiple (a) and single CSD (b). Different timings in glucose and oxygen consumption cause a transient decrease in the ratio and a later increase above the theoretical value of 6. CSD: cortical spreading depression; CMR: cerebral metabolic rate.

together with neuronal release and consumption of lactate are plotted.

Discussion

Measured data could be explained only if the following three requirements are met: (1) glycogen is rapidly metabolized to ATP in astrocytes, thus saving more blood-borne glucose for neurons, (2) astrocytes do not consume lactate, (3) neurons do consume lactate but only if extracellular lactate levels are more than 80% above normal. This theoretical framework also provides insight into how anaerobic glycolysis and oxidative phosphorylation are coupled during both increased and reduced energy demand.

The role of lactate in brain metabolism is subject of an ongoing discussion. Lactate is produced from glucose via anaerobic glycolysis. Lactate can then either be oxidized to pyruvate and as such used for oxidative ATP production or washed out of the brain via the blood stream (presumably with the support of astrocytes). In order to explain our measurements of substrate concentrations during CSD (Figure 1), we had to assume that neurons resort to lactate consumption only at highly elevated extracellular lactate levels. This hypothesis is supported by many other in vivo data.

There is indeed strong evidence that the brain switches from a net producer to a net consumer of lactate provided that plasma lactate levels are high. Quistorff et al.[30] reviewed studies that measured arterio-venous differences of lactate concentrations during physical exercise and accordingly, during periods of elevated arterial lactate concentrations. In all studies cited in their review, net uptake of lactate by the brain occurred only when arterial plasma levels were high (>3 mM compared to 1 mM under normal conditions). This is a strong indication that, under conditions of increased blood lactate levels, lactate could be used as an alternative oxidative fuel, as stated by Boumezbeur et al.[31] "plasma lactate may be a significant net fuel for brain metabolism under conditions in which plasma lactate is elevated." This would result in sparing glucose utilization, which is corroborated by reductions of cerebral metabolic rate of glucose (CMR_{glc}) observed by Wyss et al.[32] when plasma lactate levels were elevated by more than 300%. In the present study, we did not measure the arterial plasma lactate level. The amount of cerebral lactate release during CSD is not sufficient to modify arterial plasma lactate levels.[33] But we measured significant increases of the cerebral extracellular lactate level during CSD. Given that there is a positive correlation of plasma and brain lactate levels, as observed by magnetic resonance spectroscopy,[31] and that at high plasma lactate levels there is an instantaneous equilibration between plasma and brain lactate,[34] the assumption that

utilization of lactate is driven by the extracellular level of lactate is consistent with the conclusions based on increased plasma lactate levels. In particular, our model predicts that neurons consume lactate only when extracellular lactate levels in brain tissue are elevated to ~180% of the baseline. Even then, however, neurons produced more lactate than they used during the period of increased energy demand by CSD. This could be the reason for eluding direct in vivo evidence of neuronal use of lactate up to now.

Furthermore, although in our model at the beginning we did not assume that astrocytes could not use lactate, the measured data were not consistent with astrocytic lactate consumption, which agrees with in vivo observations of Bouzier et al.[35] This does not imply that there is no uptake of lactate by astrocytes, but only that astrocytes do not use lactate as energy substrate. Astrocytes do probably contribute to lactate clearance from the brain.[36] In our model, this process is part of the removal of lactate from brain to blood (k_{LP}, see Figure 2(a)). In agreement with our results, Cruz et al.[33] also reported a net efflux of lactate from brain during CSD and Ackermann and Lear[37] during activation. Thus, under normal conditions, i.e. at normal plasma and/or extracellular lactate levels, the brain is a net producer of lactate.

Another intriguing aspect of brain metabolism has long been the changes in the CMR_{O2}/CMR_{glc} ratio during activation. The theoretical value of 6 has been either not met[38] or exceeded,[39] thus leading to opposite conclusions that either anaerobic glycolysis or oxidative phosphorylation is the main process for ATP production. Full oxidative phosphorylation includes two steps, one taking place after the other: first, glycolysis (and glycogenolysis in astrocytes) to produce glucose-6-phosphate, and second, oxidative phosphorylation of glucose-6-phosphate in the TCA cycle. During the first step, CMR_{glc} is increased while CMR_{O2} remains unchanged; during the second step, CMR_{O2} is increased. Since the first step occurs temporally before the second, the CMR_{O2}/CMR_{glc} ratio is transiently decreased (in accordance with the observations of Fox et al.[38]). Note that oxygen supply was not limited in the model and therefore the observed CMR_{O2}/CMR_{glc} ratio decrease was not due to limited oxygen availability but due to limited glucose (i.e. pyruvate) availability for oxidative phosphorylation by the mitochondria. Thereafter, the CMR_{O2}/CMR_{glc} ratio transiently increased (as observed by Madsen et al.[39]). This time course is well described by our model and we conclude that determination of the CMR_{O2}/CMR_{glc} ratio after activation critically depends on the time of the measurement, which can explain the apparent contradictive results found in the literature.

Despite this temporal aspect, we clearly find that, overall, i.e., when considering the whole period of increased energy demand, oxidative phosphorylation is the main process for ATP production, in agreement with other reports.[39,40] The relative amount of anaerobic glycolysis compared to oxidative phosphorylation is in fact, during periods of increased energy demand, very close to that during resting conditions. This indicates that energy supply, both during large energy demand and at rest, is primarily covered by oxidative metabolism even if the balance is transiently shifted to anaerobic glycolysis.

Finally, regulation of cerebral energy supply not only involves responses to short periods of increased demand but also includes the adjustment of substrate fluxes to match supply and demand during longer periods of altered cellular activity. After a single CSD we observe a state of reduced energy demand that lasts for about 60 min (thorough discussion of this result can be found in Supplementary material S3). Since glycogen stores are refilled at 40 min, this time is long enough for a new steady state of substrate fluxes to evolve. The comparison of the rate constants before and 45 min after CSD indicates that a reduction of energy demand (here by 23%, P_x) is primarily accompanied by reduction of glucose transport from blood to tissue (K_1 is reduced by 25%) and only secondarily by reduction of hexokinase activity (k_3 is reduced by 7.6%) and oxidative ATP production (k_{OXY} is reduced by 1.5%). A direct consequence of this scenario is the decrease of extracellular glucose levels, which was directly measured using mircodialysis (Figure 1(d)). The reduction of glucose transport from blood to tissue is further supported by a reduction of blood flow (Figure 1(d)). This leads to the conclusion that substrate fluxes, during times of reduced energy demand, are predominantly regulated by glucose transporters, while hexokinase activity controls the increase in energy supply during transient periods of elevated demand.

Modeling of brain metabolism

Brain metabolism critically depends on species, anesthesia, body temperature, blood pressure, plasma glucose and lactate concentrations, etc. and moreover shows high spatio-temporal variations. Furthermore, it is difficult to translate in vitro findings to the in vivo situation. The experimental data that constitute the basis of our model were recorded simultaneously in vivo, thereby reducing any uncertainties in space, time, and animal conditions. In our approach, we aimed to explain the experimental data with a model as simple as possible and as complex as necessary, i.e. with the lowest number of parameters. We started with single-cell-type model (with and without glycogen) and failed to explain the data. A two-cell type model without glycogen also failed. The successful version includes

two cell types, one with glycogen stores. Our findings, in terms of glycogen, mostly agree with the conclusions by DiNuzzo et al.:[28,41] astrocytic consumption of glycogen during activation alters glucose kinetics such that more blood-borne glucose is preserved for neurons.

Other models of brain metabolism have been published, supporting and disapproving lactate shuttling from astrocytes to neurons, considering or neglecting glycogen. Compared to our version these models have a much higher complexity with a much higher number of model parameters and most importantly experimental input to these models was derived from various in vivo and in vitro data performed in different conditions (see literature[42–44]). Our model derives from one single complete set of data. It conserves mass fluxes, complies with steady-state conditions, and reacts self-consistently to changes in ATP levels. Thus, it depicts a relatively simple but realistic scenario of substrate fluxes during increased energy demand.

Conclusion

We combined in vivo experimental data with a mass-conserving theoretical model to describe the metabolic response to CSD quantitatively. This led to significant conclusions about brain energy metabolism in general. The roles of oxidative phosphorylation relative to non-oxidative metabolism of glucose critically depend on the time point of the response to increased ATP demand. Rapid production of ATP in response to instant increased need is primarily controlled by hexokinase and mitochondrial breakdown of glucose, whereas down-regulation of ATP production in conditions of lower needs is mostly controlled by reduced blood-to-brain transport. Glycogen supports astrocytic energy supply to spare blood-borne glucose for neurons. Lactate is used to produce ATP only by neurons, and only provided extracellular lactate levels are highly increased.

Funding

The author(s) disclosed receipt of the following financial support for the research, authorship, and/or publication of this article: This work was supported by the Humboldt Foundation (fellowship for postdoctoral researchers) to DF.

Acknowledgements

The authors thank Prof. Bernd Neumaier for providing us the PET tracers and Prof. Günter Mies for critically reading the manuscript.

Declaration of conflicting interests

The author(s) declared no potential conflicts of interest with respect to the research, authorship, and/or publication of this article.

Authors' contributions

D Feuerstein performed experiments, analyzed data, developed theoretical model, wrote manuscript. H Backes developed theoretical model, performed model calculations, analyzed data, wrote manuscript. M Gramer performed experiments, developed setup for simultaneous speckle/PET data acquisition, analyzed data. M Takagaki performed surgery and experiments. P Gabel performed experiments. T Kumagai performed surgery and experiments. R Graf designed experiments.

Supplementary material

Supplementary material for this paper can be found at http://jcbfm.sagepub.com/content/by/supplemental-data

References

1. Clarke DD and Sokoloff L. Circulation and energy metabolism of the brain. In: Siegel GJ, Agranoff BW, Albers RW, et al. (eds) *Basic neurochemistry: Molecular, cellular and medical aspects*. New York, NY: Lippincott-Raven, 1999, pp.637–669.
2. Pellerin L and Magistretti PJ. Glutamate uptake into astrocytes stimulates aerobic glycolysis: a mechanism coupling neuronal activity to glucose utilization. *Proc Natl Acad Sci* 1994; 91: 10625–10629.
3. Dienel GA. Brain lactate metabolism: the discoveries and the controversies. *J Cereb Blood Flow Metab* 2012; 32: 1107–1138.
4. Dreier JP. The role of spreading depression, spreading depolarization and spreading ischemia in neurological disease. *Nat Med* 2011; 17: 439–447.
5. Lauritzen M, Dreier JP, Fabricius M, et al. Clinical relevance of cortical spreading depression in neurological disorders: migraine, malignant stroke, subarachnoid and intracranial hemorrhage, and traumatic brain injury. *J Cereb Blood Flow Metab* 2011; 31: 17–35.
6. Leão AAP. Spreading depression of activity in the cerebral cortex. *J Neurophysiol* 1944; 7: 359–390.
7. Somjen GG. Mechanisms of spreading depression and hypoxic spreading depression-like depolarization. *Physiol Rev* 2001; 81: 1065–1096.
8. Grafstein B. Mechanism of spreading cortical depression. *J Neurophysiol* 1956; 19: 154–171.
9. Jones D, Parkin M, Langemann H, et al. On-line monitoring in neurointensive care: enzyme-based electrochemical assay for simultaneous, continuous monitoring of glucose and lactate from critical care patients. *J Electroanal Chem* 2002; 538–539: 243–252.
10. Reivich M, Kuhl D, Wolf A, et al. The [18F]fluorodeoxyglucose method for the measurement of local cerebral glucose utilization in man. *Circ Res* 1979; 44: 127–137.
11. Dunn AK, Bolay H, Moskowitz MA, et al. Dynamic imaging of cerebral blood flow using laser speckle. *J Cereb Blood Flow Metab* 2001; 21: 195–201.
12. Gramer M, Feuerstein D, Steimers A, et al. Device for simultaneous positron emission tomography, laser speckle imaging and RGB reflectometry: validation and application to cortical spreading depression and brain ischemia in rats. *Neuroimage* 2014; 94: 250–262.

13. Strong AJ, Bezzina EL, Anderson PJB, et al. Evaluation of laser speckle flowmetry for imaging cortical perfusion in experimental stroke studies: quantitation of perfusion and detection of peri-infarct depolarisations. *J Cereb Blood Flow Metab* 2006; 26: 645–653.
14. Feuerstein D, Parker KH and Boutelle MG. Practical methods for noise removal: applications to spikes, non-stationary quasi-periodic noise, and baseline drift. *Anal Chem* 2009; 81: 4987–4994.
15. Adachi K, Cruz NF, Sokoloff L, et al. Labeling of metabolic pools by [6-14C]glucose during K(+)-induced stimulation of glucose utilization in rat brain. *J Cereb Blood Flow Metab* 1995; 15: 97–110.
16. Selman WR, Lust WD, Pundik S, et al. Compromised metabolic recovery following spontaneous spreading depression in the penumbra. *Brain Res* 2004; 999: 167–174.
17. Mutch WA and Hansen AJ. Extracellular pH changes during spreading depression and cerebral ischemia: mechanisms of brain pH regulation. *J Cereb Blood Flow Metab* 1984; 4: 17–27.
18. Mies G and Paschen W. Regional changes of blood flow, glucose, and ATP content determined on brain sections during a single passage of spreading depression in rat brain cortex. *Exp Neurol* 1984; 84: 249–258.
19. Dam M, Ori C, Pizzolato G, et al. The effects of propofol anesthesia on local cerebral glucose utilization in the rat. *Anesthesiology* 1990; 73: 499–505.
20. Cohen PJ, Wollman H, Alexander SC, et al. Cerebral carbohydrate metabolism in man during halothane anesthesia: effects of PaCO2 on some aspects of carbohydrate utilization. *Anesthesiology* 1964; 25: 185–191.
21. Gniel HM and Martin RL. Changes in membrane potential and the intracellular calcium concentration during CSD and OGD in layer V and layer II/III mouse cortical neurons. *J Neurophysiol* 2010; 104: 3203–3212.
22. Sokoloff L, Reivich M, Kennedy C, et al. The [14C]deoxyglucose method for the measurement of local cerebral glucose utilization: theory, procedure, and normal values in the conscious and anesthetized albino rat. *J Neurochem* 1977; 28: 897–916.
23. Takano T, Tian G, Peng W, et al. Cortical spreading depression causes and coincides with tissue hypoxia. *Nat Neurosci* 2007; 10: 754–762.
24. Hawkins RA, Miller AL, Nielsen RC, et al. The acute action of ammonia on rat brain metabolism in vivo. *Biochem J* 1973; 134: 1001–1008.
25. Vaishnavi SN, Vlassenko AG, Rundle MM, et al. Regional aerobic glycolysis in the human brain. *Proc Natl Acad Sci U S A* 2010; 107: 17757–17762.
26. Krivanek J. Changes of brain glycogen in the spreading EEG-depression of Leao. *J Neurochem* 1958; 2: 337–343.
27. Seidel JL and Shuttleworth CW. Contribution of astrocyte glycogen stores to progression of spreading depression and related events in hippocampal slices. *Neuroscience* 2011; 192: 295–303.
28. DiNuzzo M, Mangia S, Maraviglia B, et al. Glycogenolysis in astrocytes supports blood-borne glucose channeling not glycogen-derived lactate shuttling to neurons: evidence from mathematical modeling. *J Cereb Blood Flow Metab* 2010; 30: 1895–1904.
29. Van Hall G, Strømstad M, Rasmussen P, et al. Blood lactate is an important energy source for the human brain. *J Cereb Blood Flow Metab* 2009; 29: 1121–1129.
30. Quistorff B, Secher NH and Van Lieshout JJ. Lactate fuels the human brain during exercise. *FASEB J* 2008; 22: 3443–3449.
31. Boumezbeur F, Petersen KF, Cline GW, et al. The contribution of blood lactate to brain energy metabolism in humans measured by dynamic 13C nuclear magnetic resonance spectroscopy. *J Neurosci* 2010; 30: 13983–13991.
32. Wyss MT, Jolivet R, Buck A, et al. In vivo evidence for lactate as a neuronal energy source. *J Neurosci* 2011; 31: 7477–7485.
33. Cruz NF, Adachi K and Dienel GA. Rapid efflux of lactate from cerebral cortex during K+ -induced spreading cortical depression. *J Cereb Blood Flow Metab* 1999; 19: 380–392.
34. Knudsen GM. Blood-brain barrier transport of lactate. In: Choi Y and Gruetter R (eds) *Neural metabolism in vivo*. Springer Science+Business Media LLC, 2012, pp.755–761.
35. Bouzier AK, Thiaudiere E, Biran M, et al. The metabolism of [3-(13)C]lactate in the rat brain is specific of a pyruvate carboxylase-deprived compartment. *J Neurochem* 2000; 75: 480–486.
36. Mergenthaler P, Lindauer U, Dienel GA, et al. Sugar for the brain: the role of glucose in physiological and pathological brain function. *Trends Neurosci* 2013; 36: 587–597.
37. Ackermann RF and Lear JL. Glycolysis-induced discordance between glucose metabolic rates measured with radiolabeled fluorodeoxyglucose and glucose. *J Cereb Blood Flow Metab* 1989; 9: 774–785.
38. Fox PT, Raichle ME, Mintun MA, et al. Nonoxidative glucose consumption during focal physiologic neural activity. *Science* 1988; 241: 462–464.
39. Madsen PL, Cruz NF, Sokoloff L, et al. Cerebral oxygen/glucose ratio is low during sensory stimulation and rises above normal during recovery: excess glucose consumption during stimulation is not accounted for by lactate efflux from or accumulation in brain tissue. *J Cereb Blood Flow Metab* 1999; 19: 393–400.
40. Hall CN, Klein-Flügge MC, Howarth C, et al. Oxidative phosphorylation, not glycolysis, powers presynaptic and postsynaptic mechanisms underlying brain information processing. *J Neurosci* 2012; 32: 8940–8951.
41. DiNuzzo M, Mangia S, Maraviglia B, et al. The role of astrocytic glycogen in supporting the energetics of neuronal activity. *Neurochem Res* 2012; 37: 2432–2438.
42. Cloutier M, Bolger FB, Lowry JP, et al. An integrative dynamic model of brain energy metabolism using in vivo neurochemical measurements. *J Comput Neurosci* 2009; 27: 391–414.
43. Jolivet R, Allaman I, Pellerin L, et al. Comment on recent modeling studies of astrocyte-neuron metabolic interactions. *J Cereb Blood Flow Metab* 2010; 30: 1982–1986.
44. Mangia S, DiNuzzo M, Giove F, et al. Response to 'comment on recent modeling studies of astrocyte-neuron metabolic interactions': much ado about nothing. *J Cereb Blood Flow Metab* 2011; 31: 1346–1353.